BIOCHEMISTRY
including biophysical chemistry & molecular biology

Article

pubs.acs.org/biochemistry

# Subunit Interactions within the Carbon−Phosphorus Lyase Complex from *Escherichia coli*

Zhongjie Ren,[†] Soumya Ranganathan,[‡] Nathanael F. Zinnel,[‡] William K. Russell,[‡] David H. Russell,*[,‡] and Frank M. Raushel*[,†,‡]

[†]Department of Biochemistry & Biophysics, [‡]Department of Chemistry, Texas A&M University, College Station, Texas 77845, United States

Supporting Information

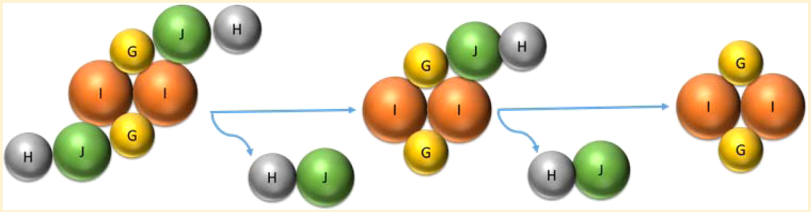


**ABSTRACT:** Phosphonates are a large class of organophosphorus compounds with a characteristic carbon−phosphorus bond. The genes responsible for phosphonate utilization in Gram-negative bacteria are arranged in an operon of 14 genes. The carbon−phosphorus lyase complex, encoded by the genes *phnGHIJKLM*, catalyzes the cleavage of the stable carbon−phosphorus bond of organophosphonates to the corresponding hydrocarbon and inorganic phosphate. Recently, complexes of this enzyme containing five subunits (PhnG-H-I-J-K), four subunits (PhnG-H-I-J), and two subunits (PhnG-I) were purified after expression in *Escherichia coli* (*Proc. Natl. Acad. Sci., U. S. A.* 2011, *108*, 11393). Here we demonstrated using mass spectrometry, ultracentrifugation, and chemical cross-linking experiments that these complexes are formed from a $PhnG_2I_2$ core that is further elaborated by the addition of two copies each of PhnH and PhnJ to generate $PhnG_2H_2I_2J_2$. This complex adds an additional subunit of PhnK to form $PhnG_2H_2I_2J_2K$. Chemical cross-linking of the five-component complex demonstrated that PhnJ physically interacts with both PhnG and PhnI. We were unable to demonstrate the interaction of PhnH or PhnK with any other subunits by chemical cross-linking. Hydrogen−deuterium exchange was utilized to probe for alterations in the dynamic properties of individual subunits within the various complexes. Significant regions of PhnG become less accessible to hydrogen/deuterium exchange from solvent within the $PhnG_2I_2$ complex compared with PhnG alone. Specific regions of PhnI exhibited significant differences in the H/D exchange rates in $PhnG_2I_2$ and $PhnG_2H_2I_2J_2K$.

Phosphorus is essential for life but the availability of this element can be limited in various ecosystems. Today, the most abundant sources of phosphorus are orthophosphate and various phosphate esters.[1] However, organophosphonates may have been the most predominant phosphorus source from the prebiotic earth.[2] In contrast to phosphate esters, which contain a hydrolyzable C−O−P bond, the C−P bond in organophosphonates is highly resistant to chemical hydrolysis, thermal decomposition, and photolysis. The C−P bond in organophosphonate-containing lipids and exopolysaccharides helps to stabilize the cell membrane in some marine organisms.[3] Organophosphonate moieties have also been employed within antibiotics, such as fosfomycin, and the herbicides phosphinothricin and phosphonothrixin.[4] Every year more than 20000 tons of phosphonates are discharged in the United States, primarily as herbicides and detergents.[5]

The bacterial C−P lyase complex catalyzes the complex biochemical pathway for the metabolism of phosphonates. and these transformations are illustrated in Scheme 1. In bacteria such as *Escherichia coli*, the catalytic machinery for the C−P lyase complex is governed by an operon of 14 genes (*phnCDEFGHIJKLMNOP*) that is up-regulated by the PhoR/PhoB two-component signaling system.[3] Four of the expressed proteins (PhnC, PhnD, PhnE, and PhnF) are necessary as regulatory or transport proteins.[6,7] Seven of the proteins (PhnG through PhnM) are critical for the enzymatic steps during the conversion of organophosphonates to phosphate,[8] and three enzymes (PhnN, PhnO, and PhnP) catalyze auxiliary reactions.[9−11]

The individual chemical reactions involved in the cleavage of the carbon phosphorus bond in methylphosphonate by the individual components of the C−P lyase complex from *E. coli* have been reconstituted in vitro.[12] PhnI, in the presence of PhnG, PhnH, and PhnL, catalyzes the displacement of adenine from ATP by methylphosphonate (MePn) to form ribose-1-methylphosphonate-5-triphosphate. In the second step, this product is hydrolyzed by PhnM to generate ribose-1-methylphosphonate-5-phosphate, and in the last step PhnJ catalyzes the cleavage of this product to form methane and ribose-1,2-cyclic phosphate-5-phosphate. PhnG, PhnH, and

**Received:** February 24, 2015
**Revised:** May 2, 2015
**Published:** May 8, 2015

ACS Publications © 2015 American Chemical Society



DOI: 10.1021/acs.biochem.5b00194
*Biochemistry* 2015, 54, 3400−3411

Scheme 1

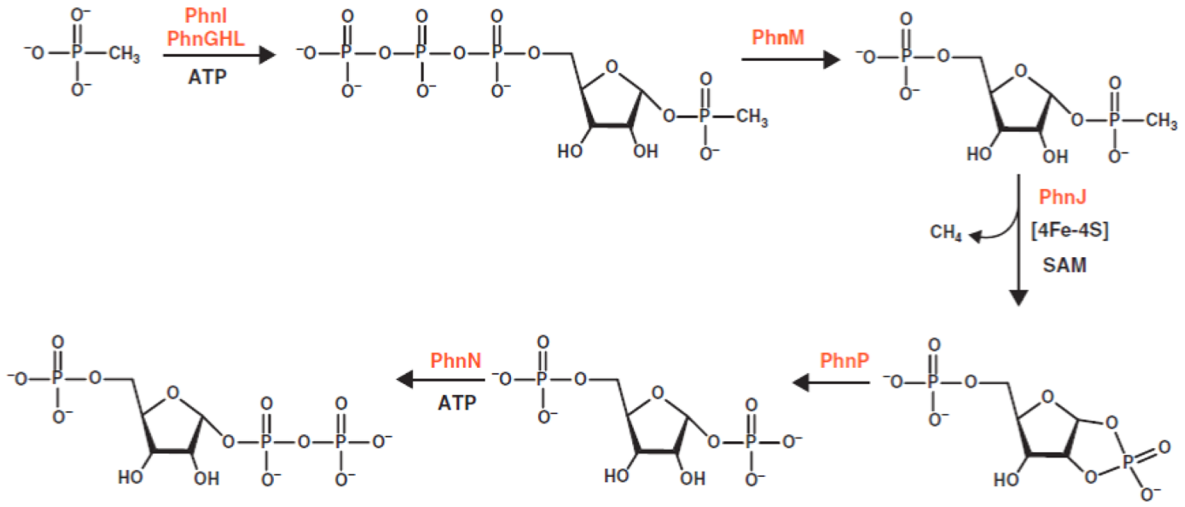


PhnM have been expressed and purified via standard methods. However, PhnI, PhnJ, PhnK, and PhnL have only been expressed and purified as glutathione S-transferase conjugates.[12] The instability of these proteins in the absence of chaperones has significantly hampered the structural elucidation of those enzymes responsible for phosphonate metabolism.

Zechel, Hove-Jensen, and colleagues have recently demonstrated that multisubunit fragments of the C−P lyase complex can be expressed from plasmids in *E. coli* and subsequently purified to apparent homogeneity.[13] Partial complexes containing PhnG and PhnI (PhnG-I); PhnG, PhnH, PhnI, and PhnJ (PhnG−H-I-J); and PhnG, PhnH, PhnI, PhnJ, and PhnK (PhnG-H-I-J-K) were expressed and purified in high yield with high solubility and stability without the need for solubility tags.[13] However, the catalytic properties, stoichiometry, and three-dimensional structural information are not currently available for any of these fragments from the C−P lyase complex. Here we use high-resolution mass spectrometry, chemical cross-linking, hydrogen/deuterium exchange, analytical ultracentrifugation, and *N*-terminal protein sequencing to structurally characterize the protein−protein interactions within the C−P lyase complex from *E. coli*.

## MATERIALS AND METHODS

**Materials.** LB broth was purchased from Research Products International Corporation. The HisTrap and gel filtration columns were obtained from GE Healthcare. Mini-PROTEAN precast gels were purchased from Bio-Rad. Bis-sulfosuccinimidyl suberate (BS3), immobilized pepsin resin, and trypsin were purchased from Thermo Scientific. The C18 reverse phase column was purchased from Waters Corporation. $D_2O$ was obtained from Cambridge Isotope Laboratories. All other buffers, purification reagents, and chemicals used in this project were purchased from Sigma/Aldrich, unless otherwise noted.

**Cloning and Expression of C−P Lyase Complexes.** DNA containing the gene for PhnG through PhnK (*his*-PhnG-H-I-J-K and PhnG-H-I-J-K-*his*) from *E. coli* was amplified from the strain BW5328/pGY3 (CGSC, Yale University). For the *his*-PhnG-H-I-J-K construct, 5′-AGCTCGTCGAT GCGACATATGCACGCAGATACCGCGACCCGCC-3′ and 5′-TCAAGTGGATCCTCAATTCTGCAAAACCGATGACACCAGCAGCTG-3′ were utilized as the forward and reverse primers, respectively. For the PhnG-H-I-J-K-*his* construct, 5′-AGCTCGTCGAT GCGACATATGCACGCAGATACCGCGACCCGCC-3′ and 5′-TCAAGTCTCGAGATTCTGCAAAACCGATGACACCAGCAGCTG-3′ were utilized as the forward and reverse primers, respectively. The polymerase chain reaction (PCR) was performed using Platinum Pfx DNA polymerase (Life Technology) and the following reaction conditions: 5 min at 95 °C, followed by 30 cycles of 30 s at 95 °C, 30 s at 66 °C, and 5 min at 72 °C. The *his*-PhnG-H-I-J-K PCR fragment was subsequently digested by the restriction enzymes Nde1 and BamH1 (New England Biolabs). The digested DNA fragment was ligated to a pET-28b vector for expression with an *N*-terminal 6x-His-tag for purification. The PhnG-H-I-J-K-*his* PCR fragment was subsequently digested by the restriction enzymes Nde1 and Xho1 (New England Biolabs). The digested DNA fragment was ligated to a pET-24b vector for expression with a C-terminal 6x-His-tag for purification. The DNA for the expression of *his*-PhnG, *his*-PhnH, *his*-PhnG-I, and PhnG-I-*his* (containing only PhnG and PhnI) and PhnG-H-I-J-*his* (containing PhnG, PhnH, PhnI, and PhnJ) was cloned as previously described.[12,13]

**Protein Purification.** The plasmids for the expression of the various complexes of C−P lyase were transformed into Rosetta2 (DE3) pLysS cells (Novagen) by electroporation and plated on LB agar. A single colony was used to inoculate 10 mL of LB medium containing 50 $\mu$g/mL kanamycin and allowed to grow overnight at 37 °C (250 rpm agitation). The 10 mL culture was subsequently used to inoculate 1 L of LB medium and incubated (250 rpm agitation) at 37 °C for 2−3 h until the $OD_{600}$ reached ~0.6. The temperature was then reduced to 18 °C and the culture induced with 0.5 mM isopropyl-$\beta$-thiogalactoside (IPTG). The cells were harvested by centrifugation after 16−18 h of incubation and then stored at −80 °C. The frozen cells were thawed and then resuspended (4:1, v/w) in buffer A (50 mM HEPES, pH 8.5, 150 mM NaCl, and 20 mM imidazole) containing 0.10 mg/mL PMSF and a protease inhibitor cocktail. The cells were disrupted by sonication, the insoluble debris was removed by centrifugation at 4 °C, and the supernatant solution applied to a 5 mL HisTrap (GE Healthcare) column. The column was pre-equilibrated with 10 column volumes of buffer A, and the proteins were eluted with a gradient of buffer B (500 mM imidazole in buffer A). The fractions were pooled and applied to a High Load 26/60 Superdex 200 prep grade gel filtration column (GE Healthcare), which was previously equilibrated with buffer C (buffer A without imidazole).



DOI: 10.1021/acs.biochem.5b00194
*Biochemistry* 2015, 54, 3400−3411

The fractions were pooled and analyzed by SDS-PAGE. Typical yields for the PhnG-H-I-J-K C−P lyase complexes were ∼30 mg/L of culture. Typical yields for the *his*-PhnG, *his*-PhnH, *his*-PhnG-I, PhnG-I-*his*, and PhnG-H-I-J-*his* fragments were ∼18 and ∼25 mg per liter of culture, respectively. The N-terminal His-tag was cleaved by Thrombin CleanCleave Kit (Sigma-Aldrich) following the manufacturer's protocol.

***N*-Terminal Protein Sequencing.** The amino acid sequence and stoichiometry of the subunits of the two protein complexes were determined by amino terminal protein sequencing using a Procise 494A protein sequencer (Applied Biosystems). Eight cycles of automated Edman degradation of the PhnG-I-*his* complex was performed. The subunit stoichiometry was calculated by comparing the relative protein concentration of each subunit after each cycle of Edman degradation.

**Analytical Ultracentrifugation.** The molecular mass and oligomeric state of three C−P lyase complexes (*his*-PhnG-I, *his*-PhnG-H-I-J, and *his*-PhnG-H-I-J-K) were characterized by sedimentation velocity using an Optima XL-A analytical ultracentrifuge (Beckman Instruments). All experiments and analyses were conducted at the University of Texas Health Science Center, San Antonio, TX. Samples of the C−P lyase complexes contained 10 mM Tris (pH 8.5), 150 mM NaCl, and 1.0 mM DTT. The protein concentrations ranged from 0.25 to 0.75 mg/mL, and the samples were centrifuged at 30000 rpm at 20 °C. The density and relative viscosity of the buffers were calculated as 1.004700 g/mL and 1.01418 mPa·s, respectively.[14] On the basis of the sequence of the C−P lyase complexes, the partial specific volume (vbar) of the protein complexes were calculated as 0.7272 mL $g^{-1}$. The absorbance of the samples was measured at 231 nm with a 50 s delay.

**ESI-MS Measurements.** ESI MS measurements were acquired with a ThermoScientific Exactive Plus EMR. In general, protein complexes were buffered with 50 mM ammonium acetate and loaded into an in-house pulled tip containing a platinum wire. All mass spectra were calibrated externally using a 1.0 $\mu$g/$\mu$L solution of cesium iodide. The protein complexes were buffered exchanged into 50 mM ammonium acetate (pH 6.8) prior to analysis using Bio-Rad Micro Bio-Spin columns. A potential of 1500−1800 V was applied to the spray ti,p and $m/z$ was scanned from 900 to 16000. Important instrument parameters used were: FT resolution was set to 17500, S-Lens RF = 200, S-Lens = 42 V, skimmer = 15 V, ion injection time was limited to 200 ms, AGC target set to 1000000, and 40 microscans were acquired. Typical acquisition times were 4 min. Source CID and HCD voltage were varied to either limit fragmentation or to promote it (see figure legends for details). The protein complex compositions and stoichiometry was determined via mass differences observed in the intact MS analysis of the protein complex. Obtained data were deconvoluted with Thermo Scientific Protein Deconvolution software. Typical settings for the deconvolution were an $m/z$ range of 2000−13000, output mass range 20000−300000, 75 ppm mass tolerance, charge state range of 4−50, four iterations, minimum adjacent charges 4−7, and a resolution of 12374 at 400m/z. Because of sample heterogeneity and the nature of the native spray analysis, it is estimated that all deconvoluted masses have an error of 400 ppm.

**Chemical Cross-Linking.** The chemical cross-linking agent BS3 was added to a solution of 20 $\mu$M *his*-PhnG-H-I-J-K (in buffer C) to a final concentration of 2.5 mM and then incubated on ice for 2 h. The reaction was quenched by Laemmli sample buffer (2% SDS, 10% glycerol, 120 mM Tris-HCl, pH 6.8) and subsequently analyzed by SDS-PAGE. The gel was stained with 3 mg/mL Coomassie brilliant blue R250 and then destained with a solution containing 30% methanol and 10% acetic acid. The sample was proteolyzed via the addition of trypsin using a previously described protocol.[15] The final samples were analyzed by LC-MS (Dionex nanoRSLC and an Orbitrap Fusion Tribrid mass spectrometer from Thermo Scientific). Briefly, 1.0 $\mu$L of the digested protein sample was loaded onto a 75 $\mu$m × 15 cm Acclaim Pepmap C18 column and eluted over 30 min with a total run time of 1 h. The eluted peptides were introduced into the mass spectrometer and analyzed using the Orbitrap (OT) mass spectrometer in positive ion mode with the following settings: resolution 120 K, scan range 400−1500 $m/z$, maximum injection time 50 ms, AGC target $2 \times 10^4$, and S-lens RF level = 60. Charge states from 2 to 7 were accepted, and targeting ions were excluded for 60 s. MS/MS data were obtained using the HCD cell and fragment masses determined using the OT mass spectrometer at a resolution of 30 K. The data were analyzed using the cross-linking identification software StavroX (version 3.4.5).[16] For the analysis of peptide masses from cross-linking experiments, a maximum mass deviation of 7 ppm and a minimal signal-to-noise ratio (S/N) of three were accepted. The mass range was set as 200−5000 Da. Decoy searches were also conducted with the same parameters using the reverse protein sequences to determine the false positive rate. The results were evaluated by the StavroX software.[16] For scores larger than 76, the false-positive rate was less than 5%. Candidate peptides with scores higher than 76 were selected and then manually checked before being assigned as positives. Additionally, carbamidomethylation of cysteine was taken into account as a fixed modification and oxidation of methionine was set as a varied modification. Up to three missed-cleavage sites were utilized during data processing.

**Hydrogen/Deuterium Exchange.** The *his*-PhnG, *his*-PhnH, and *his*-PhnG-I were concentrated to 2.5 mg/mL and the *his*-PhnG-H-I-J-K complex was concentrated to 4.5 mg/mL. Deuterated buffers were prepared by removing water from the aqueous buffer containing 50 mM HEPES (pH 8.5), 200 mM NaCl, and 2.0 mM TCEP using a centrifugal vacuum concentrator and then adding an equivalent volume of 99.9% $D_2O$ (Cambridge Isotope Laboratories, Inc.). A total of 4.0 $\mu$L of the concentrated protein sample was diluted into 36 $\mu$L of aqueous buffer for the undeuterated sample. The deuterated samples were obtained by diluting 4 $\mu$L of protein into 36 $\mu$L of the deuterated buffer (90% deuteration) for various amounts of time (4 and 10 s, 1.0, 2.0, 5.0, 15, and 30 min, and 1.0 h) at 0 °C. The deuterium exchange reaction was quenched with 60 $\mu$L of ice-cold buffer containing 3.0 M urea and 50 mM TCEP at pH 2.1 to bring the final pH of the resultant mixture to pH 2.3−2.4.[17,18] A total of 50 $\mu$L of the quenched sample was added to 50 $\mu$L of immobilized pepsin resin (Thermo Scientific, USA). The pepsin beads were preactivated by washing with 1% (v/v) TFA in water, pH 2.0. The digestion was carried out at ∼6 °C for 5 min with frequent vortexing. The solution was then transferred to a 0.22 $\mu$m Ultrafree-MC GV centrifugal filter (EMD Millipore), and the pepsin beads were removed by centrifugation at 8000 rpm for 30 s. The supernatant solution was divided into aliquots and immediately flash-frozen in liquid nitrogen and stored at −80 °C.

The subsequent analysis by mass spectrometry was performed using a Thermo Scientific Q Exactive instrument within two to three days of sample preparation. The samples were thawed on ice prior to injection to minimize back-exchange. The peptic


DOI: 10.1021/acs.biochem.5b00194
*Biochemistry* 2015, 54, 3400−3411

digests of *his*-PhnG, *his*-PhnH, *his*-PhnG-I, and *his*-PhnG-H-I-J-K were applied to a 2.1 mm × 100 mm Symmetry C18 reverse-phased column (Waters Corporation, Milford, MA) using 0.1% (v/v) formic acid in water at a flow rate of 200 μL/min. The peptides were eluted using a gradient of 8−55% acetonitrile over the course of 8 min. The solvents and column were placed in an ice-bath throughout the experiment to reduce the back-exchange of deuterons during analysis. A blank solution using acetonitrile was utilized between each sample to avoid peak carry-over between runs. The mass spectrometer was calibrated using an LTQ ESI positive ion calibration solution from Thermo Scientific, USA. The peptides were identified using the software Peptide Mapping (Thermo Scientific) with a mass tolerance of 10 ppm for the theoretical mass-to-charge ($m/z$) ratios. Oxidation of methionine was set as a possible modification. The peptides were further confirmed by LC-MS/MS analysis on an Orbitrap Fusion Tribrid mass spectrometer from Thermo Scientific as described earlier. The pepsin digestion provided sequence coverages of 88%, 83%, and 86% for the PhnG, PhnH, and PhnG-I complexes, respectively. The PhnG-H-I-J-K complex had a sequence coverage of 89% for PhnG and PhnI and 83% for PhnH.

The deuterium content and centroid values of each peptide at various time points were calculated using the software HDExaminer (Sierra Analytics, Modesto, CA). Each identified peptide was manually examined and validated. It was assumed that the maximum number of exchangeable amides in a peptide is two less than the total number of amino acids in the peptide minus any proline residues.[17−19] The shifts in the centroid values for the deuterated samples were determined using the undeuterated sample as a control. The various charge states of an individual peptide were used to calculate the deuterium level, and the values between them did not show much change. For regions of the proteins containing multiple overlapping peptides, a maximum of three overlaps encompassing the wider region were used in the analysis. The peptide exchange plots were generated using MS-Excel. The deuterated samples were not corrected for back-exchange, and all of the reactions were carried out under identical conditions.

**Homology Modeling and Secondary Structure Predictions.** The homology model for PhnK was created using the Intensive Mode of the web-based structure prediction software Phyre2[20] with the nucleotide-binding domain of a dipeptide ABC transporter (PDB id: 4FWI), which has a 32% sequence identity with PhnK. For PhnG, PhnI, and PhnJ, the homology modeling was conducted using Swiss Model[21] and the secondary structure prediction was carried out using SABLE protein structure prediction server.[22] All protein structure figures were generated using Pymol (http://www.pymol.org).

## RESULTS

**Characterization of PhnG-I.** Two different contructions were prepared for the expression of a complex that contained only PhnG and PhnI. The first of these had a polyhistidine purification tag at the *N*-terminus of PhnG, and the second had the polyhistidine tag at the *C*-terminus of PhnI. The calculated molecular masses for the subunits within these two complexes are as follows: PhnG (16 524 Da), *his*-PhnG (18 688 Da), PhnI (38 852 Da), and PhnI-*his* (39 917 Da). Both of these complexes migrated as a single peak upon elution from a calibrated Superdex 200 10/300 GL gel filtration column (GE Heathcare) (data not shown), and the approximate molecular mass was determined to be 140 ± 26 kDa.

The molecular mass for the *his*-PhnG-I complex was also determined by using analytical ultracentrifugation and ESI mass spectrometry. For the *his*-PhnG-I complex, the sedimentation coefficient ($S_w^{20}$) of 5.89 S corresponds to an apparent molecular mass of 115.8 ± 1.7 kDa at a protein concentration of 0.25 mg/mL. The sedimentation velocity experiment was also conducted at a protein concentration of 0.75 mg/mL and a van Holde−Weischet analysis indicated that the oligomeric state of *his*-PhnG-I did not change at the higher protein concentration. Under native ESI conditions, the *his*-PhnG-I complex exhibited charge states in the gas phase with a range of +21 to +25 and a mass of 115300 Da (Figure 1). CID fragmentation of the *his*-PhnG-I complex resulted in the loss of a PhnG monomer and a mass corresponding to $PhnGI_2$ (96600 Da), as well as the appearance of a mass at 56000 Da that corresponds to PhnGI, indicating that PhnG and PhnI form a heterodimer (Supporting Information Figure S1).

The stoichiometry of the PhnG-I-*his* complex was addressed by *N*-terminal amino acid sequence analysis. After seven rounds of *N*-terminal amino acid sequencing, the ratio of the amino acids specific for PhnG to that for PhnI averaged 0.9 ± 0.1. Therefore, the apparent stoichiometry of the two subunits contained within the PhnG-I-*his* complex is ∼1:1. Given the mass of the *his*-PhnG-I complex determined from analytical ultracentrifugation (115800 Da) and ESI mass spectrometry (115770 Da), it is concluded that the stoichiometry of the complex containing only PhnG and PhnI is $PhnG_2I_2$.

**SDS Electrophoresis of $PhnG_2I_2$.** The subunit composition of the $PhnG_2I_2$ complex was confirmed by SDS-PAGE, and the identity of each band was verified by in-gel digestion with trypsin and mass spectroscopy (Figure 2). The intensity of the Coomassie Blue staining for each of the two separated subunits of $PhnG_2I_2$ was measured using a Gel Doc EZ System densitometer (BioRad). For the $PhnG_2I_2$-*his* complex, the relative staining intensity for subunits PhnG and PhnI-*his* was 1.00:1.22 and 1.00:1.07 for *his*-$PhnG_2I_2$. When the *his*-tag was removed by proteolysis with thrombin, the relative staining intensity for these two subunits was similar (1.00:1.17). Because the molecular mass ratios for the two subunits are 1.00:2.42 (for PhnG and PhnI-*his*) and 1.00:2.09 (for *his*-PhnG and PhnI), PhnG stains approximately twice as dense per amino acid than does PhnI under these conditions.

**Characterization of PhnG-H-I-J.** The complex that contains subunits PhnG, PhnH, PhnI, and PhnJ was cloned with a polyhistidine tag at the *C*-terminus of PhnJ. This complex migrated as a single homogeneous peak after elution from a gel filtration column (data not shown). The approximate molecular mass for this complex was determined to be 243 ± 38 kDa using a calibrated Superdex 200 10/300 GL gel filtration column (GE Heathcare). Two species were identified by ultracentrifugation at a protein concentration of 0.25 mg/mL. The major component (79.9%) exhibited an $S_w^{20}$ value of 9.43 S and an estimated molecular mass of 218.8 ± 7.4 kDa. The minor component (19.1%) had an $S_w^{20}$ value of 7.90 S with an estimated molecular mass of 191.0 ± 9.1 kDa. The sedimentation velocity experiments were also conducted at a higher protein concentration (0.75 mg/mL), and these experiments indicated that the PhnG-H-I-J-*his* complex aggregated at the higher protein concentration during the ultracentrifugation process.

The subunit composition of the PhnG-H-I-J-*his* complex was confirmed by SDS-PAGE, and the identity of each band was verified by in-gel digestion with trypsin and mass spectroscopy (Figure 2). The intensity of the Coomassie Blue staining for each



DOI: 10.1021/acs.biochem.5b00194
*Biochemistry* 2015, 54, 3400−3411

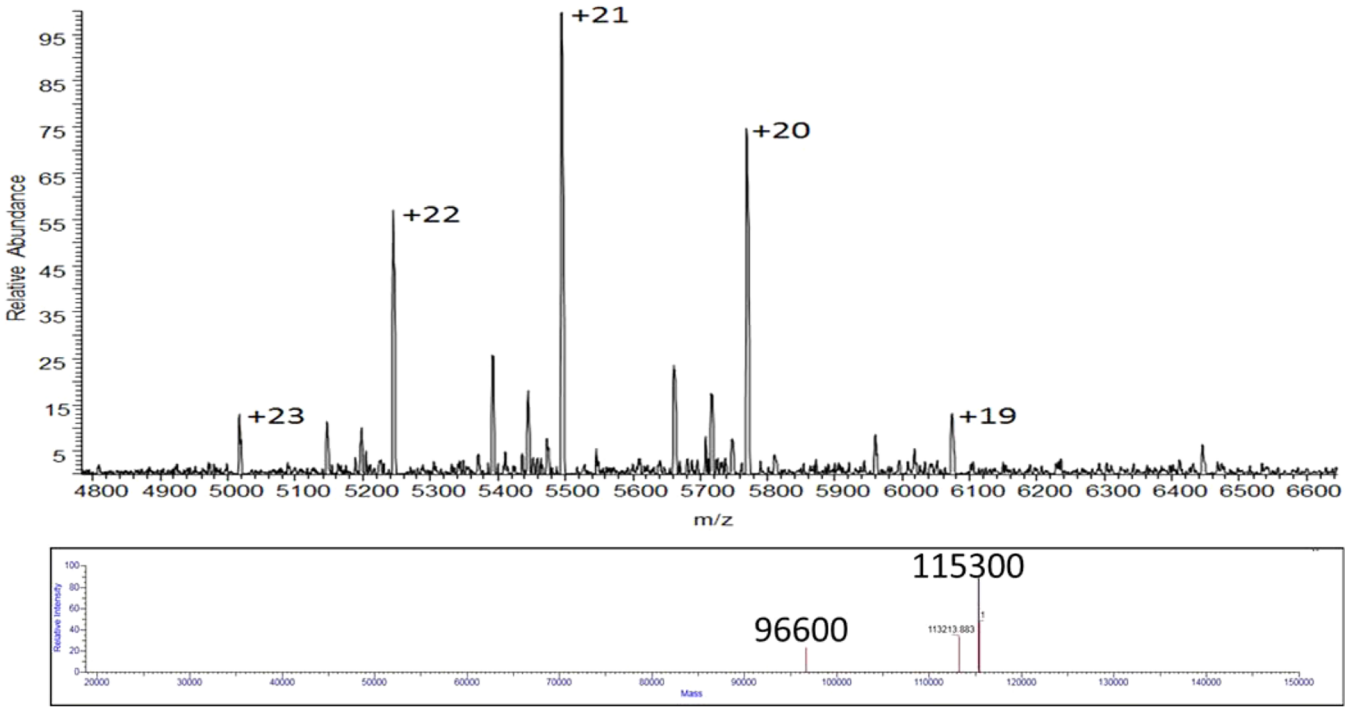


**Figure 1.** Native ESI of the $PhnG_2I_2$ complex. The upper figure is the raw data obtained using 75 V of energy in the HCD cell and 50 V of energy in the source region. The bottom figure is the deconvoluted data using the isotope clusters from the upper mass spectrum of the complex, which represents the +19 to +23 charge states of the complex.

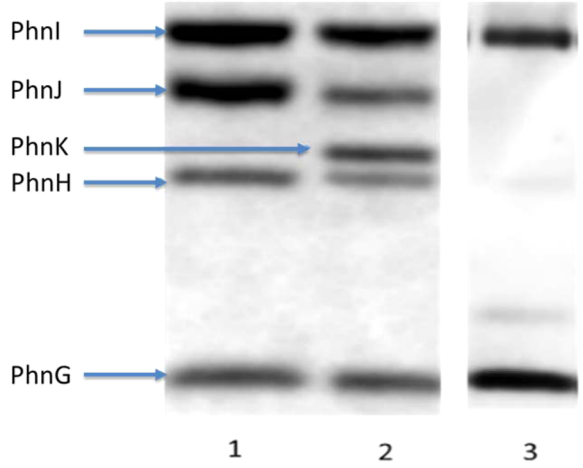


**Figure 2.** SDS-PAGE separation of the subunits contained within the C−P lyase complexes from *E. coli*. Lane 1: *his*-$PhnG_2I_2$. Lane 2: *his*-$PhnG_2H_2I_2J_2$. Lane 3: *his*-$PhnG_2H_2I_2J_2K$. All protein complexes were diluted to 2 mg/mL in sample buffer (65.8 mM Tris-HCl, pH 6.8, 2.1% SDS, 26.3% (w/v) glycerol, 0.01% bromophenol blue) and loaded onto a Bio-Rad mini-protean precast gel. The gel was stained by Coomassie Brilliant Blue and the relative intensity of each band quantified using a Gel Doc EZ System densitometer (BioRad).

of the separated subunits was measured, and the relative staining intensities for subunits PhnG, PhnH, PhnI, and PhnJ-*his* are listed in Table 1. From the relative staining intensities for PhnG and PhnI in this complex (1.19−1.28), we can conclude that these two subunits are in a ratio of 1:1 because this is essentially the same ratio as found in the $PhnG_2I_2$ complex (1.17).

Under native ESI conditions, the parent mass of the PhnG-H-I-J-*his* complex was measured to be approximately 222200 Da (Figure 3). In an effort to elucidate the subunit composition of

**Table 1. Relative Staining Intensities in PhnG-H-I-J and PhnG-H-I-J-K**

| | PhnG | PhnH | PhnI | PhnJ |
|---|---|---|---|---|
| PhnG-H-I-J | 27.6 | 11.2 | 35.4 | 25.9 |
| PhnG-H-I-J-*his* | 26.0 | 13.5 | 31.0 | 29.5 |
| PhnG-H-I-J-K | 25.4 | 11.8 | 35.8 | 27.0 |
| PhnG-H-I-J-K-*his* | 22.7 | 11.3 | 38.0 | 27.9 |
| *his*-PhnG-H-I-J-K | 28.5 | 9.3 | 37.5 | 24.8 |
| ave | 26.0 | 11.4 | 35.5 | 27.0 |

this complex, the collisional energy was raised as high as 200 V and the resulting deconvoluted fragment masses of 197900, 166300, 144000, 111100, 94500, and 55600 were obtained (Supporting Information Figure S2). These fragments correspond to the sequential loss of PhnH (21.0 kDa), PhnJ-*his* (32.8 kDa), PhnH (21.0 kDa), PhnJ-*his* (31.7 kDa), PhnG (16.5 kDa), and PhnI (38.9 kDa). PhnGI is the smallest fragment that was observed. These results are consistent with the formation of PhnHJ and PhnGI heterodimers in the complex and that the overall composition for this complex is $PhnG_2H_2I_2J_2$.

**Characterization of PhnG-H-I-J-K.** The complex composed of PhnG through PhnK was cloned and subsequently expressed with a polyhistidine tag at either the *N*-terminus of PhnG or the *C*-terminus of PhnK. Both of these complexes migrated through a calibrated gel filtration column as a single peak (data not shown) with an estimated molecular mass of 285 ± 46 kDa. The subunit compositions of the two PhnG-H-I-J-K complexes were confirmed by SDS-PAGE, and the identity of each band was verified by in-gel digestion with trypsin and mass spectroscopy (Figure 2). To estimate the stoichiometry of the subunits contained within these two complexes, the relative Coomassie Blue staining intensities for PhnG, PhnH, PhnI, and PhnJ were compared to the relative staining intensities for these same subunits in the complex that contains only four subunits (Table 1).


DOI: 10.1021/acs.biochem.5b00194
*Biochemistry* 2015, 54, 3400−3411

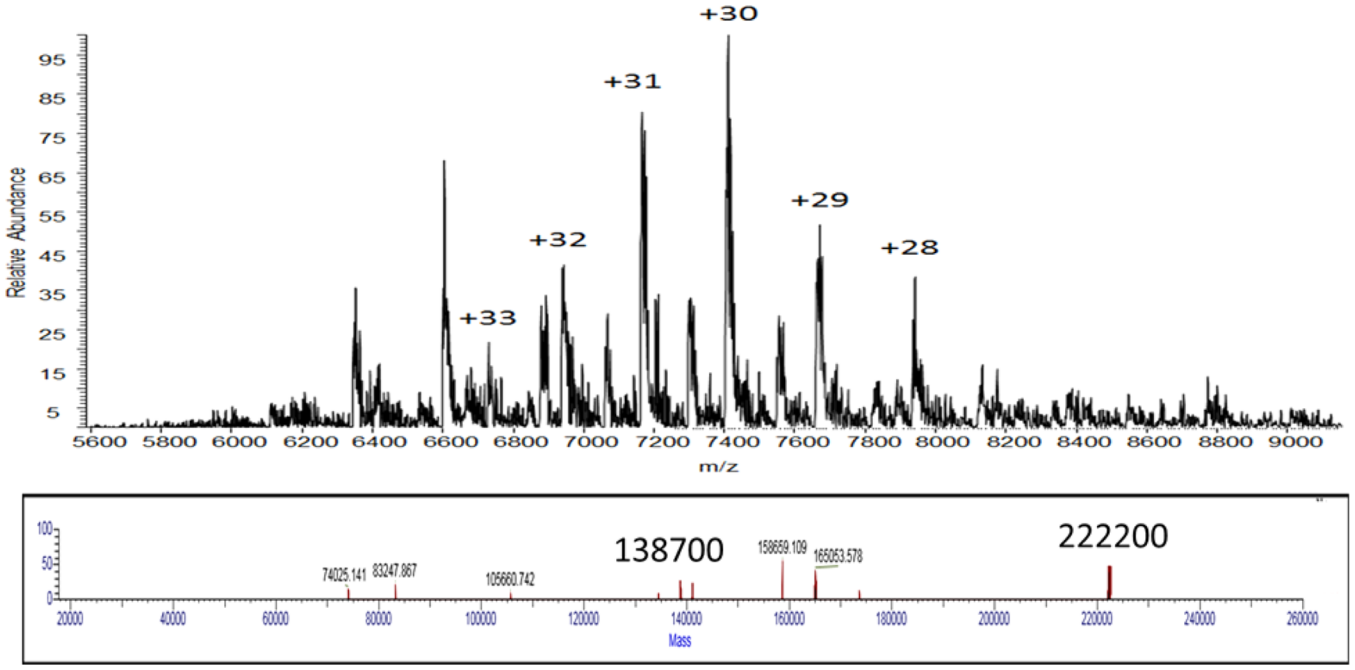


**Figure 3.** Native ESI of the $PhnG_2H_2I_2J_2$ complex. The upper figure is the raw data obtained using 10 V of energy in the HCD cell and 10 V of energy in the source region. The bottom figure is the deconvoluted data utilizing the isotope clusters from the upper mass spectrum of the complex, which represents the +28 to +33 charge states of the complex.

Within experimental error, the relative staining intensities for PhnG, PhnH, PhnI, and PhnJ contained within the $PhnG_2H_2I_2J_2$ complexes matched those contained within either of the complexes that contained all five subunits. Therefore, the $PhnG_2H_2I_2J_2$ core is retained within the two complexes that now contain PhnK.

The molecular mass of the PhnG-H-I-J-K complex was estimated using analytical ultracentrifugation. At a protein concentration of 0.25 mg/mL, the $S_w^{20}$ value was determined to be 8.94 S for the PhnG-H-I-J-K-*his* complex with a calculated molecular mass of 236.9 ± 8.3 kDa. The sedimentation velocity experiments were also conducted at a protein concentration of 0.75 mg/mL and a van Holde–Weischet analysis indicated that the oligomeric state of PhnG-H-I-J-K-*his* was constant at the two protein concentrations. The mass of the PhnG-H-I-J-K-*his* complex was also determined using ESI mass spectrometry. Under native ESI conditions, the PhnG-H-I-J-K-*his* complex enters the gas phase with charge states of +30 to +36, corresponding to a mass of 249700 (Figure 4), a value that is consistent with that determined by analytical ultracentrifugation. Using 75 V of source fragmentation energy and 45 V in the HCD cell, the mass at 249200 most likely represents the $PhnG_2H_2I_2J_2K$-*his* complex (calculated mass = 245144) and that at 221300 represents the $PhnG_2H_2I_2J_2$ complex (calculated mass = 216234) and the loss of PhnK-*his* (calculated mass = 28910). The mass at 196234 represents the loss of PhnHJ (calculated mass = 52741) to give $PhnG_2HI_2JK$ (calculated mass = 192403). The mass at 168598 represents the $PhnG_2HI_2J$ complex with the loss of PhnK (Supporting Information Figure S3).

**Structural Analysis by Chemical Cross-Linking.** The contact regions for interaction of the subunits contained within the $PhnG_2H_2I_2J_2K$ complex were probed by chemical cross-linking. Cross-linking was initiated with the homobifunctional reagent bis-sulfosuccinimidyl suberate (BS3) that can form a linkage of up to 11.4 Å between the $\varepsilon$-amino groups of lysine residues or the free amino group of the *N*-terminus.[23] The products of the cross-linking reactions with $PhnG_2H_2I_2J_2K$-*his* were separated by SDS-PAGE, and the results are presented in Figure 5. Four prominent high molecular mass cross-linked protein complexes of approximately 47 (band 1), 70 (band 2), 87 (band 3), and 110 kDa (band 4) were formed after incubation with BS3. Two bands of higher molecular mass at approximately 125 and 165 kDa were also formed but are less distinct. The cross-linked proteins were excised from the gel and subjected to in-gel digestion with trypsin and characterized by LC-ESI/MS. On the basis of the mass spectrometry data, the 47 kDa band contains one copy each of PhnG (17 kDa) and PhnJ (31 kDa), the 70 kDa band contains one copy each of PhnI (39 kDa) and PhnJ, and the 87 kDa band contains one copy each of PhnG, PhnI, and PhnJ. The bands at 110, 125, and 165 kDa contain mixtures of PhnG, PhnI, and PhnJ. No cross-linked proteins were identified to contain PhnH or PhnK.

The cross-linked proteins were excised, proteolyzed with trypsin, and then analyzed by LC-ESI-MS/MS to identify the specific cross-linking sites. The purified peptides were subjected to high-energy collision dissociation (HCD). A representative example of an MS/MS spectrum of a triply charged ion at $m/z$ 1004.16 (corresponding to an $M + H^+ = 3010.46$) is provided in Figure 6. The daughter ion spectrum exhibited most of the y-ion series for two peptides from PhnG ($\beta$-peptide, residues 89–95) and PhnJ ($\alpha$-peptide, residues 2–18). The y16$\beta$ and y5$\alpha$ ions indicate that Lys-89 of PhnG and the *N*-terminus of PhnJ are covalently linked to one another. A similar analysis was conducted to identify all of the other cross-linked peptides, and the identity of the cross-linked peptide pairs are presented in Table 2.

In addition to the intermolecular cross-links between different protein subunits, there were several intramolecular cross-links contained within PhnI and PhnJ. In all of the cross-linking experiments, only peptides from PhnG, PhnI, or PhnJ were identified. There was no trace of PhnH or PhnK in the cross-linked proteins. However, further analysis of the ESI-MS data identified several internally cross-linked peptides and individual lysine residues within PhnH and PhnK that were labeled with the


DOI: 10.1021/acs.biochem.5b00194
*Biochemistry* 2015, 54, 3400–3411

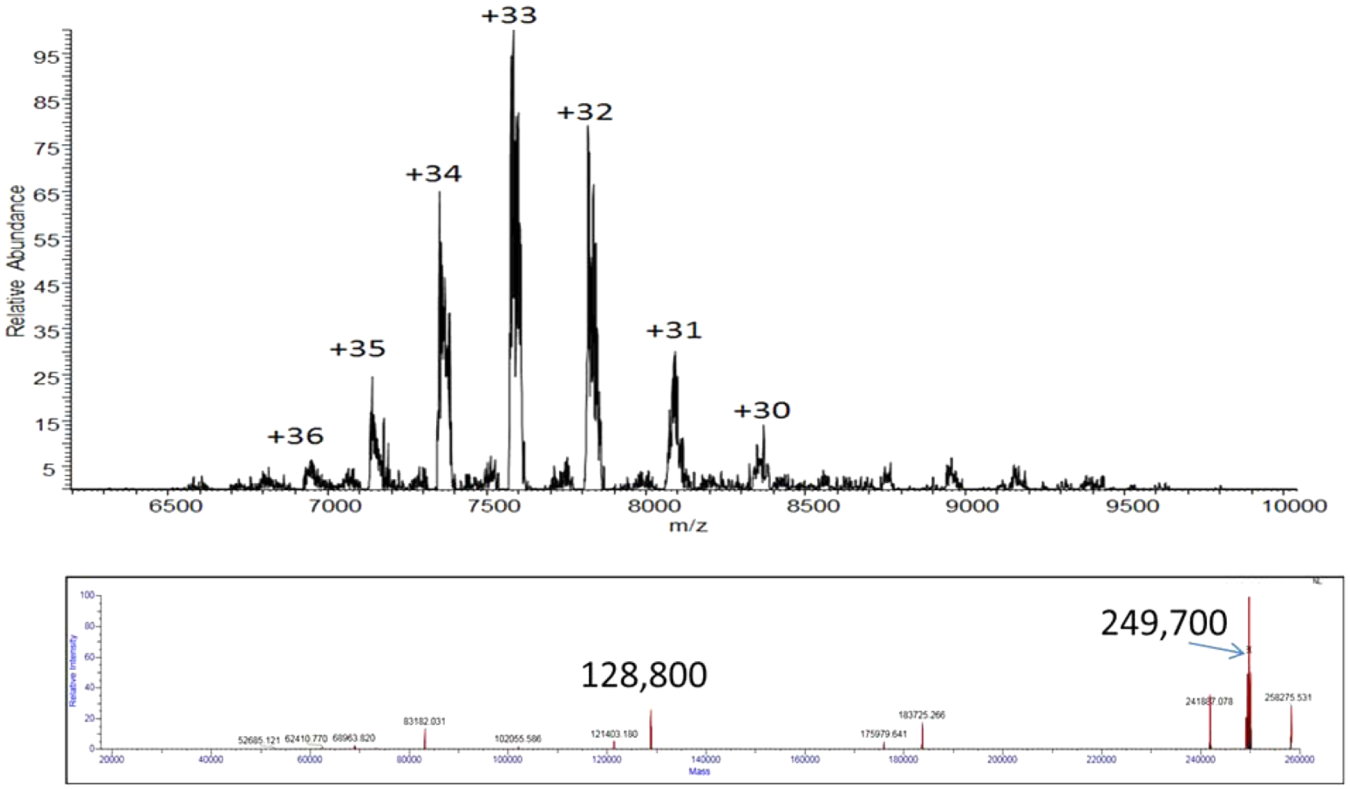


**Figure 4.** Native ESI of the $PhnG_2H_2I_2J_2K$ complex. The upper figure is the raw data obtained using 13 V of collision energy in the HCD cell and 10 V of energy in the source region. The bottom figure is the deconvoluted data utilizing the isotope clusters from the upper mass spectrum of the complex, which represents the +30 to +36 charge states of the complex.

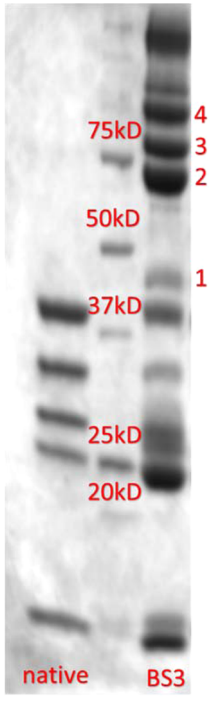


**Figure 5.** SDS-PAGE of the BS3-initiated cross-linking of those proteins contained within the various carbon−phosphorus lyase complexes. The left lane represents the separation of the subunits contained within the $PhnG_2H_2I_2J_2K$ complex prior to the addition of BS3. The middle lane is a standard molecular mass protein ladder (Bio-Rad). The rightmost lane represents the separation of cross-linked proteins after the addition of BS3 to the $PhnG_2H_2I_2J_2K$ complex. Four prominent cross-linked bands were labeled as 1, 2, 3, and 4 from the bottom to the top.

cross-linking reagent. For example, Lys-38 from PhnH was derivatized with BS3. In PhnK, the *N*-terminus, Lys-127, and Lys-220 were labeled with BS3 and an internal cross-link was identified between Lys-19 and Lys-49.

**Structural Analysis by Hydrogen/Deuterium Exchange.** Hydrogen/deuterium exchange experiments were carried out on PhnG, $PhnG_2I_2$, and $PhnG_2H_2I_2J_2K$ from the C−P lyase complex in an attempt to determine those regions of PhnG that are most affected by the association with PhnI. It was assumed that those portions of PhnG that interact directly with PhnI will exhibit a change in the rate of H/D exchange in either $PhnG_2I_2$ or $PhnG_2H_2I_2J_2K$ relative to the H/D exchange profile for PhnG alone. Reduced rates of H/D exchange may also be observed for those portions of PhnG that become more structured in either of these two complexes than in the isolated subunit alone. A difference of 10% or more in the exchange rate between any two protein complexes is considered significant. The overall coverage of peptides from PhnG that were detected by mass spectrometry in all three complexes was approximately 87%. The time course for the exchange of deuterium from solvent incorporated into the peptide $^{68}$TRAAVRLTDGTLGYS$^{82}$ from PhnG is presented in Figure 7. The time courses for H/D exchange within PhnG alone indicate that many regions of the protein undergo H/D exchange very rapidly. This is especially true for those regions of PhnG that extend from residues 28−79 and from residues 116−124 (Figure 8). All of the peptides identified for PhnG, $PhnG_2I_2$, and $PhnG_2H_2I_2J_2K$ exhibit EX2 kinetics for deuterium uptake.[24−27] Bimodal isotopic distribution spectra, which indicate the presence of local or global unfolding through EX1 kinetics, were not observed for any of the peptides of PhnG or PhnI.[24−26]

There are significant differences in the rates of deuterium exchange for those peptides from PhnG when this protein is



DOI: 10.1021/acs.biochem.5b00194
*Biochemistry* 2015, 54, 3400−3411

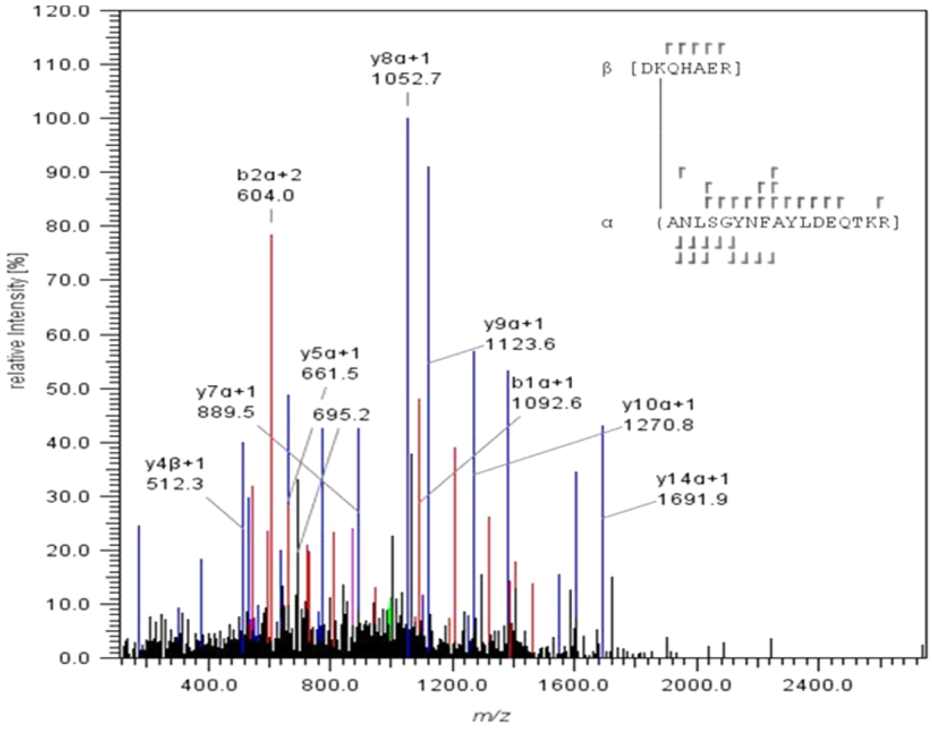


**Figure 6.** ESI-MS/MS analysis of the cross-linked peptides contained within the $PhnG_2H_2I_2J_2K$ complex. The peptide $^{88}$DKHAER$^{94}$- from PhnG and the peptide $^{2}$ANLSGNYFAYLDEQTKR$^{18}$ were cross-linked through Lys-89 from DKHAER and the *N*-terminus of ANLSGNYFAYLDEQTKR.

**Table 2. Identification of Specific Crosslinking Site of PhnG-H-I-J-K C−P Lyase Complex**[a]

| Band | M+H$^+$ | Deviation (ppm) | Sequence 1 | Protein 1 | Sequence 2 | Protein 2 |
|---|---|---|---|---|---|---|
| Band 1 | 3010.45 | -2.65 | $^{88}$DKQHAER$^{94}$ | PhnG | $^{2}$ANLSGYNFAYLDEQTKR$^{18}$ | PhnJ |
| | 2838.42 | -0.88 | $^{84}$NFFKR$^{88}$ | PhnJ | $^{2}$ANLSGYNFAYLDEQTKR$^{18}$ | PhnJ |
| Band 2 | 2501.29 | 2.34 | $^{84}$NFFKR$^{88}$ | PhnJ | $^{7}$GGEKAIDAAHALQESR$^{22}$ | PhnI |
| | 3214.42 | -1.95 | $^{1}$MYVAVKGGEK$^{10}$ | PhnI | $^{274}$QQSEAKNQ$^{281}$ | PhnJ |
| | 2857.42 | -3.37 | $^{1}$mYVAVK$^{6}$ | PhnI | $^{2}$ANLSGYNFAYLDEQTKR$^{18}$ | PhnJ |
| | 1930.02 | 1.53 | $^{84}$NFFKR$^{88}$ | PhnJ | $^{1}$MYVAVKGGEK$^{10}$ | PhnI |
| | 2838.42 | 1.09 | $^{84}$NFFKR$^{88}$ | PhnJ | $^{2}$ANLSGYNFAYLDEQTKR$^{18}$ | PhnJ |
| Band 3 | 2501.29 | 0.65 | $^{84}$NFFKR$^{88}$ | PhnJ | $^{7}$GGEKAIDAAHALQESR$^{22}$ | PhnI |
| | 3010.47 | 1.68 | $^{88}$DKQHAER$^{94}$ | PhnG | $^{2}$ANLSGYNFAYLDEQTKR$^{18}$ | PhnJ |
| | 3137.47 | -3.92 | $^{-1}$MMHADTATR$^{8}$ | PhnG | $^{196}$MDMmPALQLFGAGREKR$^{212}$ | PhnJ |
| | 2167.06 | -0.97 | $^{274}$QQSEAKNQ$^{281}$ | PhnJ | $^{1}$mYVAVKGGEK$^{10}$ | PhnI |
| | 2838.42 | 1.09 | $^{84}$NFFKR$^{88}$ | PhnJ | $^{2}$ANLSGYNFAYLDEQTKR$^{18}$ | PhnJ |
| Band 4 | 3010.47 | 1.68 | $^{88}$DKQHAER$^{94}$ | PhnG | $^{2}$ANLSGYNFAYLDEQTKR$^{18}$ | PhnJ |
| | 7691.66 | -6.61 | $^{-1}$mMHADTATRQHWMSVL AHSQPAELAAR$^{27}$ | PhnG | $^{41}$EMPMPYGWGTGGIQLTASVIGESD VLKVIDQGADDTTNAVSIR$^{81}$ | PhnJ |
| | 2501.28 | 0.65 | $^{84}$NFFKR$^{88}$ | PhnJ | $^{7}$GGEKAIDAAHALQESR$^{22}$ | PhnI |
| | 1930.02 | -2.17 | $^{84}$NFFKR$^{88}$ | PhnJ | $^{1}$MYVAVKGGEK$^{10}$ | PhnI |
| | 2682.31 | -2.83 | $^{84}$NFFKR$^{88}$ | PhnJ | $^{2}$ANLSGYNFAYLDEQTK$^{17}$ | PhnJ |

[a]m: oxidized form of methionine.

contained within the $PhnG_2I_2$ or $PhnG_2H_2I_2J_2K$ complexes. These differences are graphically depicted in the representative times courses for comparable peptides in Figure 8. For the peptides that encompass residues 16−23, 28−36, and 98−111, there are essentially no differences in the time courses for the uptake of deuterium by PhnG alone and PhnG contained within the $PhnG_2I_2$ complex. These results are in stark contrast to the significant differences in the exchange profiles for peptides that encompass residues 47−79 and 68−97 (Figure 8).

The H/D exchange profiles for the PhnG and PhnI subunits contained within the $PhnG_2I_2$ and $PhnG_2H_2I_2J_2K$ complexes are quite similar to one another (Figure 9). For PhnG, there are virtually no differences in the exchange rates for portions of the protein when this complex is embedded in either $PhnG_2I_2$ or $PhnG_2H_2I_2J_2K$. For PhnI, the only regions exhibiting differential deuterium exchange profiles between the two complexes are the peptides contained within PhnI that encompass residues from 33−41, 81−85, and 109−130 (Figure 9). These peptides show slightly more protection in the $PhnG_2H_2I_2J_2K$ complex than in the $PhnG_2I_2$ complex.

H/D exchange analysis of PhnH alone was carried out and compared with the peptides from PhnH obtained from the



DOI: 10.1021/acs.biochem.5b00194
*Biochemistry* 2015, 54, 3400−3411

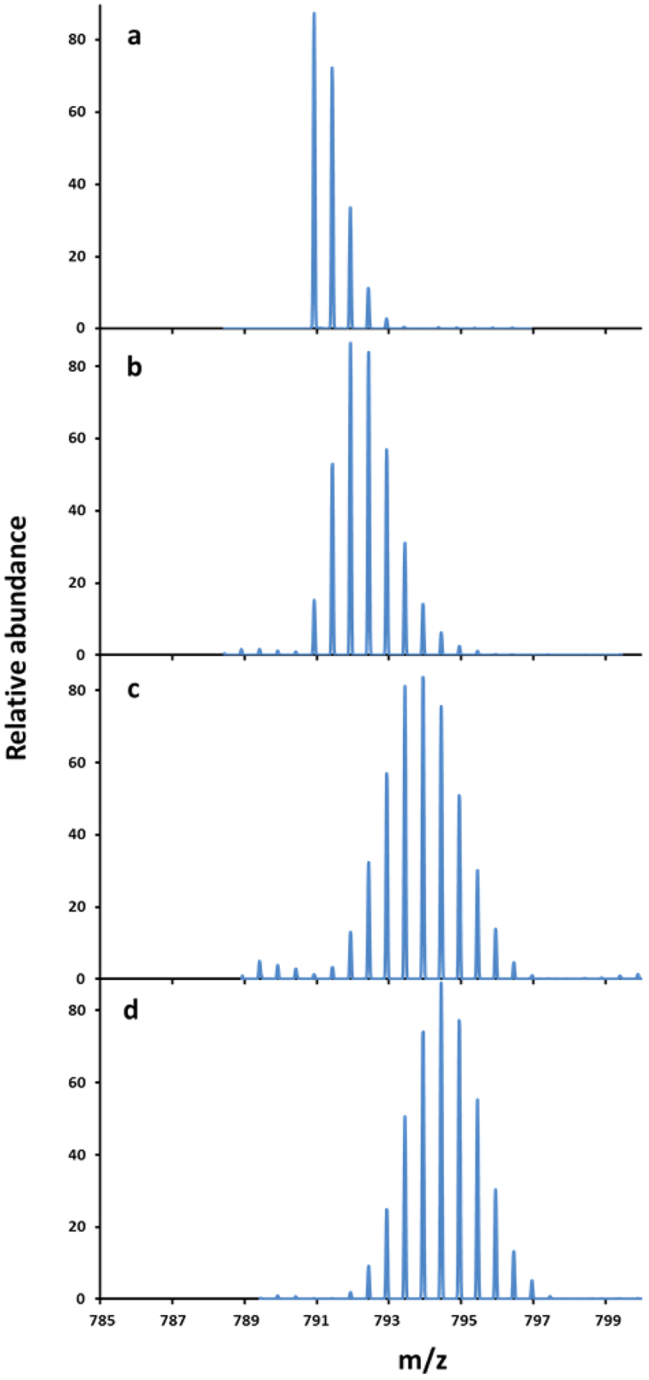


**Figure 7.** Time course for the uptake of deuterium by the peptide $^{68}$TRAAVRLTDGTLGYS$^{82}$ from PhnG as measured by ESI-MS after 0, 4 s, 5 min, and 1 h.

$PhnG_2H_2I_2J_2K$ complex to help identify those regions of PhnH that undergo structural variations upon complex formation. A total of 23 common peptides, spanning 83% of PhnH, were identified. From the deuterium uptake plots for the PhnH peptides in the individual subunit and the $PhnG_2H_2I_2J_2K$ complex, many regions along the entire length of PhnH are more protected in the $PhnG_2H_2I_2J_2K$ complex (Supporting Information Figure S4). The *N*-terminal region of PhnH, which comprises the dimerization interface in the crystal structure of PhnH, is represented by the peptides encompassing residues 6−18, 7−18, 19−24, and 19−31. This region exhibits significant

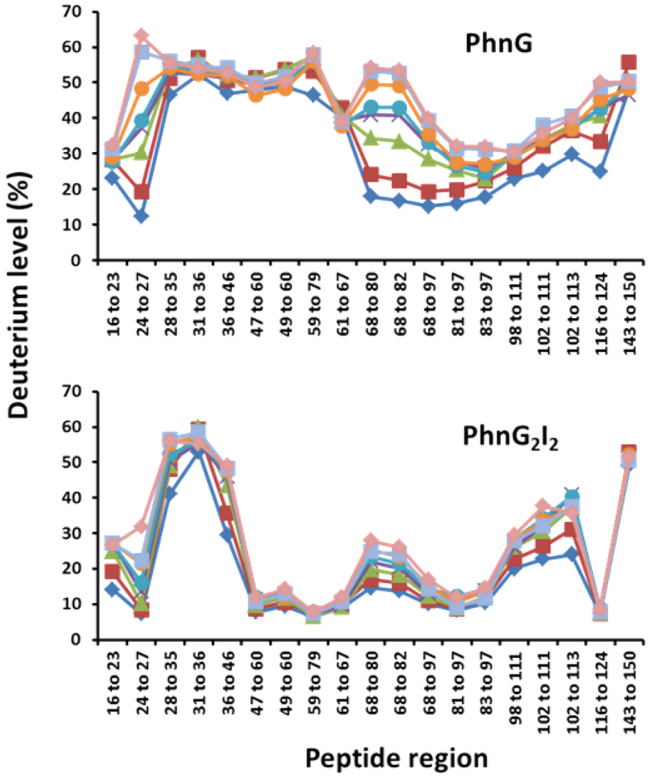


**Figure 8.** Differential deuterium exchange for the peptides contained within PhnG alone and the same peptide contained within $PhnG_2I_2$. The incubation times are as follows: 4 s (◆), 10 s (■), 1 min (▲), 2 min (□), 5 min (●), 15 min (●), 30 min (■), 60 min (◆).

reduction in deuterium exchange in the $PhnG_2H_2I_2J_2K$ complex as compared to the individual subunit of PhnH. A major difference in deuterium exchange profile is also observed in the region connecting $\alpha$-helix D with a disordered loop and stretches up to $\beta$-strand $\beta$5 for the peptides spanning residues 110−123 (peptides 107−122 and 110−123) (Supporting Information Figures S4 and S5). A high degree of differential exchange is also observed in the region extending from residues 136−146 as illustrated by the peptides $^{136}$LRLTGAG$^{142}$, $^{136}$LRLTGAGIAE$^{145}$, and $^{136}$LRLTGAGIAEE$^{146}$ (Supporting Information Figure S4). This region extends from $\beta$-strand $\beta$6 and connects through a disordered loop region to $\beta$-strand $\beta$7 (Supporting Information Figure S5). Finally, the C-terminal region of PhnH, illustrated by the peptides encompassing residues 157−173, 159−173, and 183−194 are more protected in the complex compared to the PhnH alone (Supporting Information Figure S4).

## DISCUSSION

**Stoichiometry of the C−P Lyase Complexes.** Three different protein complexes from the carbon−phosphorus lyase enzyme were expressed, purified, and characterized by gel electrophoresis, analytical ultracentrifugation, *N*-terminal protein sequencing, and high-resolution mass spectrometry. For the complex that contains only PhnG and PhnI, the results are consistent with an equal mixture of the two subunits and an overall stoichiometry of $PhnG_2I_2$. In the complex that contains these two subunits, in addition to PhnH and PhnJ, the results are consistent with a stoichiometry of $PhnG_2H_2I_2J_2$. For the complex that contains five different subunits, the complex contains two copies of PhnG, PhnH, PhnI, and PhnJ, plus a single copy of PhnK ($PhnG_2H_2I_2J_2K$). These results suggest that PhnG and


DOI: 10.1021/acs.biochem.5b00194
*Biochemistry* 2015, 54, 3400−3411

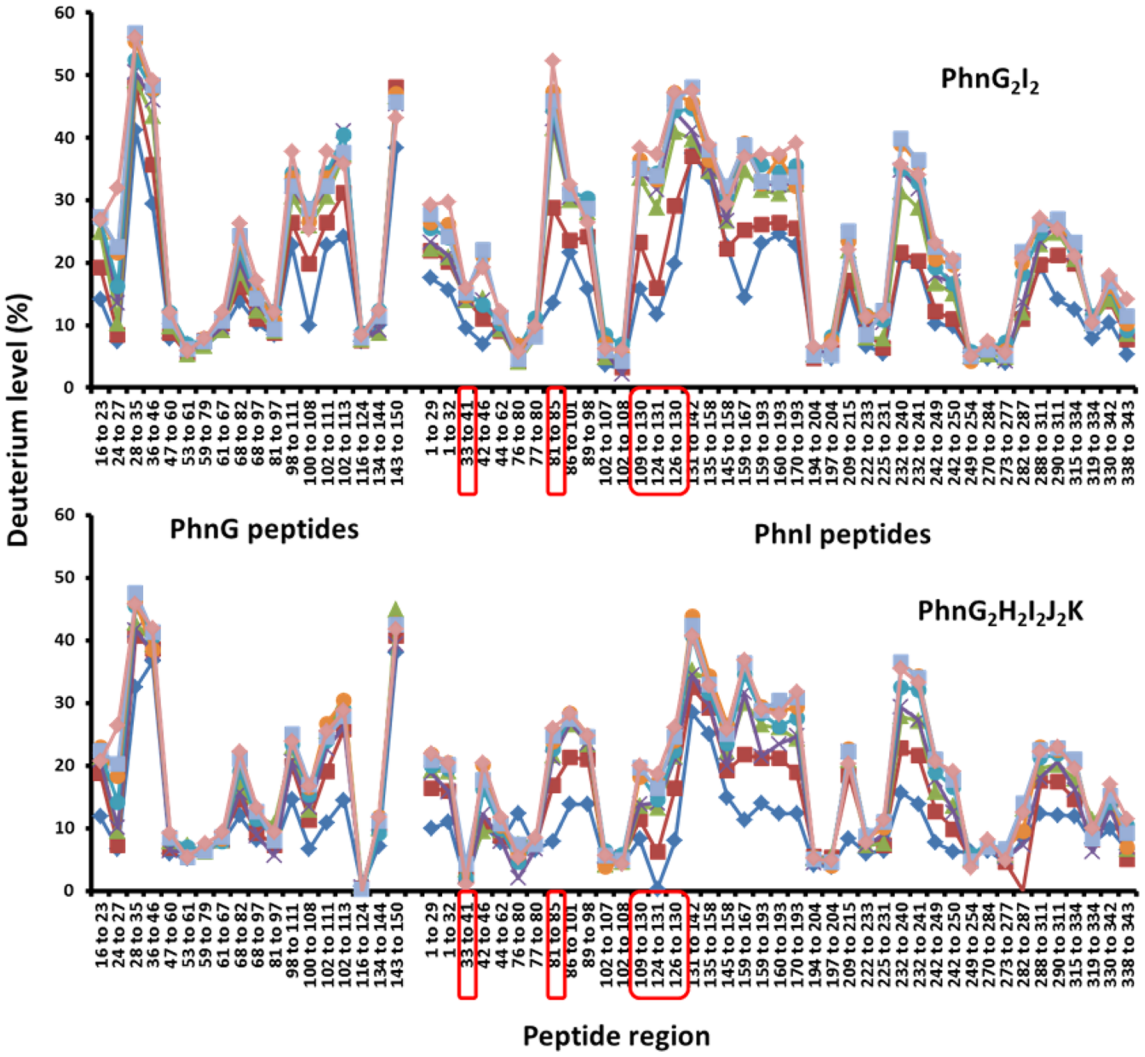


**Figure 9.** Differential deuterium exchange for the peptides contained within PhnG and PhnI for the complexes PhnG$_2$I$_2$ and PhnG$_2$H$_2$I$_2$J$_2$K. The peptides differing in exchange pattern between the two complexes are highlighted in red. The incubation times are as follows: 4 s (◆), 10 s (■), 1 min (▲), 2 min (□), 5 min (●), 15 min (●), 30 min (■), 60 min (◆).

PhnI associate to form a central heterodimeric core (PhnG$_2$I$_2$) that is required prior to the binding of two additional copies each of PhnH and PhnJ (PhnHJ) to facilitate the assembly of PhnG$_2$H$_2$I$_2$J$_2$. The largest complex is subsequently formed by the binding of a single copy of PhnK. The proposed assembly pathway for the formation of the PhnG$_2$H$_2$I$_2$J$_2$ and the PhnG$_2$H$_2$I$_2$J$_2$K complexes is further supported by the mass spectrometry results where individual subunits are progressively dissociated from the central core complex. With the PhnG$_2$H$_2$I$_2$J$_2$ complex, we observed the sequential dissociation of PhnH, PhnJ, PhnH, PhnJ, PhnG, and PhnI.

**Chemical Cross-linking.** Chemical cross-linking experiments were conducted to identify those subunits that are physically able to contact one another, and these results are graphically illustrated in Figure 10. Using PhnG$_2$H$_2$I$_2$J$_2$K, we demonstrated that subunit contacts occur between PhnG and PhnJ and between PhnJ and PhnI. PhnG and PhnI must further interact with one another because a PhnG$_2$I$_2$ complex can be isolated. Unfortunately, no cross-links could be identified between PhnH or PhnK and any other subunit. This result must reflect the fact that the *N*-terminus and the available lysine residues within these two proteins are insufficiently close to the appropriate residues contained within PhnG, PhnI, or PhnJ. We did, however, identify an internal cross-link between two lysine residues within PhnK and labeling of single lysine residues in both PhnH (Lys-38) and PhnK (Lys-127 and Lys-220).

**Hydrogen/Deuterium Exchange.** The assembly of multiprotein complexes was further addressed by measuring the rates of exchange of hydrogen and deuterium into the backbone of PhnG and PhnI from solvent. For PhnG alone, about 40% of the protein backbone undergoes deuterium exchange in a very short time (<10 s). This result demonstrates that significant portions of PhnG alone are highly dynamic and likely to be unstructured. Some of these regions become more structured upon interaction with PhnI. This is particularly true for that portion of the protein that extends from Val-47 through Leu-67 (Figure 8). However, further differences are not observed for PhnG within the PhnG$_2$H$_2$I$_2$J$_2$K complex but significant differences in the H/D exchange rates are observed for PhnI in certain regions when the PhnG$_2$I$_2$ complex is compared with the PhnG$_2$H$_2$I$_2$J$_2$K complex (Figure 9). Similar structural transitions are often found in multiprotein complexes and in intrinsically disordered proteins that undergo synergistic folding in the presence of their binding partners.[28,29]



DOI: 10.1021/acs.biochem.5b00194
*Biochemistry* 2015, 54, 3400−3411

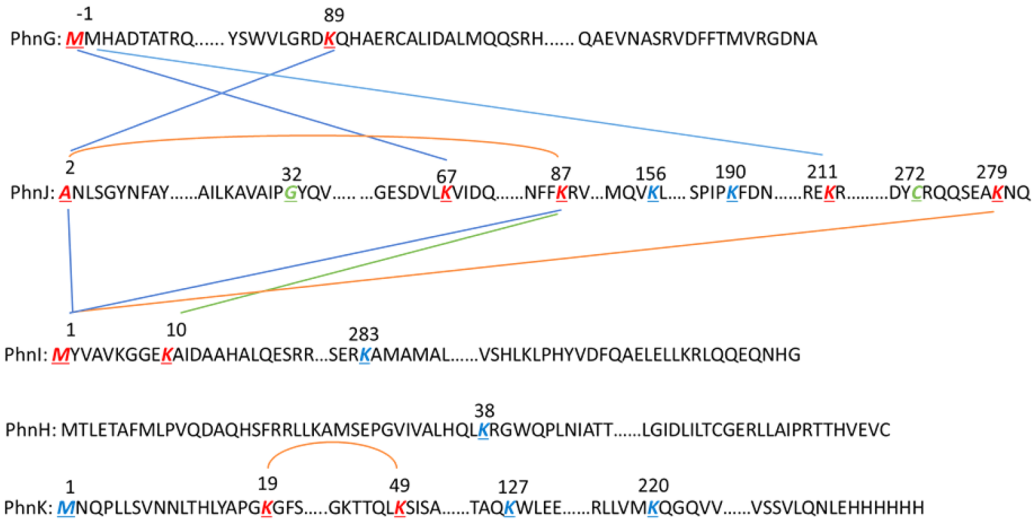


**Figure 10.** Cross-linking map of the $PhnG_2H_2I_2J_2K$ complex. All of the cross-linked residues are highlighted in red, while all of the residues that participate in a monolinkage are highlighted in blue. Two residues that were reported to be key residues within the active site of PhnJ (Gly-32 and Cys-272) are highlighted in green. The cross-linking bonds are depicted as straight lines between different cross-linking sites. The internal cross-linked bonds are presented as a curve connecting two lysine residues.

The N-terminal dimerization interface of PhnH is altered in the $PhnG_2H_2I_2J_2K$ complex. This may indicate a loss in the interaction of the PhnH monomer with another PhnH. The structural change near the dimer interface region may also imply the binding of PhnH with another subunit in the $PhnG_2H_2I_2J_2K$ complex. The crystal structure of PhnH shows the formation of a large hydrophobic pocket on the surface of each monomer as the result of dimerization by the N-terminal ends of $\beta$-strands $\beta$4 (91−94), $\beta$5 (110−121), and $\beta$8 (166−173).[30] Interestingly almost all of the regions other than the N-termini of $\beta$-strand $\beta$4 become more protected in the complex. This clearly indicates the change in the hydrophobic pocket region within the $PhnG_2H_2I_2J_2K$ complex. The C-terminal region spanning residues 185−194 also become more protected in the complex. This indicates the possible role of this region involved in subunit interactions in the complex.

**Low Resolution Structural Model.** The results obtained from the mass spectrometry and chemical cross-linking experiments can be used to propose a low-resolution model for the assembly of the C−P lyase complex (Scheme 2). In this model,

**Scheme 2**

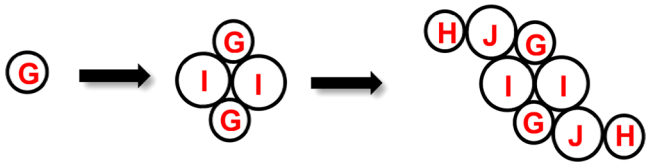


a heterodimeric core complex is formed from the association of two copies each of PhnI and PhnG. This complex serves as a platform for the further addition of two copies each of PhnH and PhnJ. Cross-linking experiments demonstrate the physical interaction between PhnI and PhnJ, but we were unable to obtain evidence for the association of PhnH with any other protein. However, we have assumed that PhnH must interact with PhnJ because both proteins are apparently required for elaboration of the $PhnG_2I_2$ core.

The closest sequence homologues for PhnG, PhnI, and PhnJ were found to be the putative Trp repressor protein (PDB id: 3KOR), carboxymethyl-2-hydroxymuconate semialdehyde dehydrogenase (PDB id: 2D4E), and PhnH (PDB id: 2FSU), respectively. However, the sequence identities of these proteins to their closest identified homologues are less than 20%, and so a reliable homology model could not be built for any of these proteins. However, it is quite interesting that the closest structural model for PhnJ is PhnH. The secondary structural predications for PhnG, PhnI, and PhnJ are presented in Supporting Information Figure S6. The predicted secondary structures are consistent with the results of H/D exchange. With PhnG, the region with the most rapid H/D exchange rate (residues 28−61) is predicted to be mostly unstructured or $\beta$-strands. For PhnI contained within $PhnG_2I_2$ and $PhnG_2H_2I_2J_2K$, most of the dynamic regions are also predicted to be unstructured or $\beta$ strands.

Lys-89 from PhnG was shown to be a cross-linking site between PhnG and PhnJ. The H/D exchange results showed a dramatic change of the exchange rate on Lys-89 when PhnG is in the $PhnG_2H_2I_2J_2K$ complex. Unfortunately, the cross-linking sites for PhnG and PhnI are all located close the *N*-terminus, which is not covered by the H/D exchange experiments. It is possible that the *N*- and *C*-terminal regions of PhnH are involved in the interaction with PhnJ based on the differential deuterium exchange analysis of PhnH. The peptides which contain Lys-23 ($^{19}$RRLLKA$^{24}$ and $^{19}$RRLLKAMSEPGVI$^{31}$) exchange at a much slower rate in the $PhnG_2H_2I_2J_2K$ complex than in PhnH itself, and the region containing Lys-38 does not show a significant difference between the two protein complexes. Because there are no cross-linked peptides for PhnH, we are not able to identify the regions involved in interaction with PhnJ or any other subunit in the complex.

The homology model of PhnK indicates that residues Lys-19 and Lys-49, which are internally cross-linked, are separated by a distance of about 20 Å (Supporting Information Figure S7). The cross-linking agent is ~11 Å in length. This indicates that the region containing these two lysine residues must come closer together in the complex. Although the lysine residues in the homology model of PhnK appear to be on the protein surface, no peptides of PhnK were cross-linked to any other subunit. It is currently unclear how PhnK binds to the $PhnG_2H_2I_2J_2$ complex or why only one copy of PhnK binds to an apparently dimeric complex. What is obviously required is the crystallization and three-dimensional structure determination of these complexes.



DOI: 10.1021/acs.biochem.5b00194
*Biochemistry* 2015, 54, 3400−3411

## ■ ASSOCIATED CONTENT

### Supporting Information

ESI mass spectra for the fragmentation of complexes $PhnG_2I_2$, $PhnG_2H_2I_2J_2$ and $PhnG_2H_2I_2J_2K$. H/D exchange data for PhnH, the structure of PhnH, secondary structure predictions for PhnG, PhnI, and PhnJ, and the homology model for PhnK. The Supporting Information is available free of charge on the ACS Publications website at DOI: 10.1021/acs.biochem.5b00194.

## ■ AUTHOR INFORMATION


### Corresponding Authors

*For F.M.R.: phone, 979-845-3373; fax, 979-845-9452; e-mail, raushel@tamu.edu.

*For D.H.R.: phone, 979-845-3345; fax, 979-845-9485; e-mail, russell@chem.tamu.edu.


### Notes

The authors declare no competing financial interest.

## ■ ACKNOWLEDGMENTS

We thank John Patrick (Texas A&M University) for valuable assistance with the ESI experiments and Professor Vicki Wysocki and Royston Quintyn (Ohio State University) for valuable discussions and assistance with ESI-MS of protein complexes. We also gratefully acknowledge Jamie K. Humphries and ThermoScientific for providing access to the Exactive mass spectrometer used in these studies. We are grateful to Dr. Larry Dangott of the Protein Chemistry Laboratory at Texas A&M University for his assistance with the H/D exchange experiments.

## ■ REFERENCES


(1) Hsieh, Y. J., and Wanner, B. L. (2010) Global regulation by the seven-component Pi signaling system. *Curr. Opin. Microbiol. 13*, 198−203.

(2) Jia, Y., Lu, Z., Huang, K., Herzberg, O., and Dunaway-Mariano, D. (1999) Insight into the mechanism of phosphoenolpyruvate mutase catalysis derived from site-directed mutagenesis studies of active site residues. *Biochemistry 38*, 14165−14173.

(3) McGrath, J. W., Chin, J. P., and Quinn, J. P. (2013) Organophosphonates revealed: new insights into the microbial metabolism of ancient molecules. *Nature Rev. Microbiol. 11*, 412−419.

(4) Kononova, S. V., and Nesmeyanova, M. A. (2002) Phosphonates and their degradation by microorganisms. *Biochemistry (Moscow) 67*, 184−195.

(5) Kamat, S. S., and Raushel, F. M. (2013) The enzymatic conversion of phosphonates to phosphate by bacteria. *Curr. Opin. Chem. Biol. 17*, 589−596.

(6) Chen, C. M., Ye, Q. Z., Zhu, Z. M., Wanner, B. L., and Walsh, C. T. (1990) Molecular biology of carbon−phosphorus bond cleavage. Cloning and sequencing of the phn (psiD) genes involved in alkylphosphonate uptake and C−P lyase activity in *Escherichia coli* B. *J. Biol. Chem. 265*, 4461−4471.

(7) Gebhard, S., and Cook, G. M. (2008) Differential regulation of high-affinity phosphate transport systems of *Mycobacterium smegmatis*: identification of PhnF, a repressor of the phnDCE operon. *J. Bacteriol. 190*, 1335−1343.

(8) Yakovleva, G. M., Kim, S. K., and Wanner, B. L. (1998) Phosphate-independent expression of the carbon−phosphorus lyase activity of *Escherichia coli*. *Appl. Microbiol. Biotechnol. 49*, 573−578.

(9) Hove-Jensen, B., McSorley, F. R., and Zechel, D. L. (2011) Physiological role of PhnP-specified phosphoribosyl cyclic phosphodiesterase in catabolism of organophosphonic acids by the carbon−phosphorus lyase pathway. *J. Am. Chem. Soc. 133*, 3617−3624.

(10) Hove-Jensen, B., McSorley, F. R., and Zechel, D. L. (2012) Catabolism and detoxification of 1-aminoalkylphosphonic acids: *N*-acetylation by the phnO gene product. *PLoS One 7*, e46416.

(11) Hove-Jensen, B., Rosenkrantz, T. J., Haldimann, A., and Wanner, B. L. (2003) *Escherichia coli* phnN, encoding ribose 1,5-bisphosphokinase activity (phosphoribosyl diphosphate forming): dual role in phosphonate degradation and NAD biosynthesis pathways. *J. Bacteriol. 185*, 2793−2801.

(12) Kamat, S. S., Williams, H. J., and Raushel, F. M. (2011) Intermediates in the transformation of phosphonates to phosphate by bacteria. *Nature 480*, 570−573.

(13) Jochimsen, B., Lolle, S., McSorley, F. R., Nabi, M., Stougaard, J., Zechel, D. L., and Hove-Jensen, B. (2011) Five phosphonate operon gene products as components of a multi-subunit complex of the carbon−phosphorus lyase pathway. *Proc. Natl. Acad. Sci. U. S. A. 108*, 11393−11398.

(14) DemelerB. UltraScan: a comprehensive data analysis software package for analytical ultracentrifugation experiments (2005) in *Modern Analytical Ultracentrifugation: Techniques and Methods*, pp 210−229, Royal Society of Chemistry, London

(15) Shevchenko, A., Tomas, H., Havlis, J., Olsen, J. V., and Mann, M. (2007) In-gel digestion for mass spectrometric characterization of proteins and proteomes. *Nature Protocols 1*, 2856−2860.

(16) Gotze, M., Pettelkau, J., Schaks, S., Bosse, K., Ihling, C. H., Krauth, F., Fritzsche, R., Kuhn, U., and Sinz, A. (2012) StavroX—a software for analyzing crosslinked products in protein interaction studies. *J. Am. Soc. Mass. Spectrom. 23*, 76−87.

(17) Bai, Y., Milne, J. S., Mayne, L., and Englander, S. W. (1993) Primary structure effects on peptide group hydrogen exchange. *Proteins 17*, 75−86.

(18) Englander, S. W., and Kallenbach, N. R. (1983) Hydrogen exchange and structural dynamics of proteins and nucleic acids. *Q. Rev. Biophys. 16*, 521−655.

(19) Walters, B. T., Ricciuti, A., Mayne, L., and Englander, S. W. (2012) Minimizing back exchange in the hydrogen exchange−mass spectrometry experiment. *J. Am. Soc. Mass. Spectrom. 23*, 2132−2139.

(20) Kelley, L. A., and Sternberg, M. J. E. (2009) Protein structure prediction on the web: a case study using the Phyre server. *Nature Protoc. 4*, 363−371.

(21) Arnold, K., Bordoli, L., Kopp, J., and Schwede, T. (2006) The SWISS-MODEL Workspace: a web-based environment for protein structure homology modeling. *Bioinformatics 22*, 195−201.

(22) Adamczak, R., Porollo, A., and Meller, J. (2005) Combining prediction of secondary structure and solvent accessibility in proteins. *Proteins: Struct., Funct., Bioinform. 59*, 467−475.

(23) Sinz, A. (2003) Chemical cross-linking and mass spectrometry for mapping three-dimensional structures of proteins and protein complexes. *J. Mass Spectrom. 38*, 1225−1237.

(24) Krishna, M. M., Hoang, L., Lin, Y., and Englander, S. W. (2004) Hydrogen exchange methods to study protein folding. *Methods (San Diego, CA, U. S.) 34*, 51−64.

(25) Weis, D. D., Wales, T. E., Engen, J. R., Hotchko, M., and Ten Eyck, L. F. (2006) Identification and characterization of EX1 kinetics in H/D exchange mass spectrometry by peak width analysis. *J. Am. Soc. Mass. Spectrom. 17*, 1498−1509.

(26) Wales, T. E., and Engen, J. R. (2006) Hydrogen exchange mass spectrometry for the analysis of protein dynamics. *Mass Spectrom. Rev. 25*, 158−170.

(27) Liyanage, R., Devarapalli, N., Puckett, L. M., Phan, N. H., Gidden, J., Stites, W. E., and Lay, J. O., Jr. (2009) Comparison of two ESI MS based H/D exchange methods for extracting protein folding energies. *Int. J. Mass Spectrom. 287*, 96−104.

(28) Demarest, S. J., Martinez-Yamout, M., Chung, J., Chen, H., Xu, W., Dyson, H. J., Evans, R. M., and Wright, P. E. (2002) Mutual synergistic folding in recruitment of CBP/p300 by p160 nuclear receptor coactivators. *Nature 415*, 549−553.

(29) Bhattacherjee, A., and Wallin, S. (2012) Coupled folding-binding in a hydrophobic/polar protein model: impact of synergistic folding and disordered flanks. *Biophys. J. 102*, 569−578.

(30) Adams, M. A., Luo, Y., Hove-Jensen, B., He, S. M., van Staalduinen, L. M., Zechel, D. L., and Jia, Z. (2008) Crystal structure of PhnH: an essential component of carbon-phosphorus lyase in *Escherichia coli*. *J. Bacteriol. 190*, 1072−1083.




DOI: 10.1021/acs.biochem.5b00194
*Biochemistry* 2015, 54, 3400−3411